ACS APPLIED MATERIALS & INTERFACES

Research Article

www.acsami.org

# Imine-Linked Polymer-Derived Nitrogen-Doped Microporous Carbons with Excellent $CO_2$ Capture Properties

Jiacheng Wang,*[,†] Irena Senkovska,[‡] Martin Oschatz,[‡] Martin R. Lohe,[‡] Lars Borchardt,[‡] Andreas Heerwig,[‡] Qian Liu,[†] and Stefan Kaskel*[,‡]

[†]State Key Laboratory of High Performance Ceramics and Superfine Microstructure, Shanghai Institute of Ceramics, 1295 Dingxi Road, Shanghai 200050, China

[‡]Department of Inorganic Chemistry, Dresden University of Technology, Bergstraße 66, 01069 Dresden, Germany

Supporting Information

**ABSTRACT:** A series of nitrogen-doped microporous carbons (NCs) was successfully prepared by direct pyrolysis of high-surface-area microporous imine-linked polymer (ILP, 744 $m^2/g$) which was formed using commercial starting materials based on the Schiff base condensation under catalyst-free conditions. These NCs have moderate specific surface areas of up to 366 $m^2/g$, pore volumes of 0.43 $cm^3/g$, narrow micropore size distributions, and a high density of nitrogen functional groups (5.58−8.74%). The resulting NCs are highly suitable for $CO_2$ capture adsorbents because of their microporous textural properties and large amount of Lewis basic sites. At 1 bar, NC-800 prepared by the pyrolysis of ILP at 800 °C showed the highest $CO_2$ uptakes of 1.95 and 2.65 mmol/g at 25 and 0 °C, respectively. The calculated adsorption capacity for $CO_2$ per $m^2$ ($\mu$mol of $CO_2/m^2$) of NC-800 is 7.41 $\mu$mol of $CO_2/m^2$ at 1 bar and 25 °C, the highest ever reported for porous carbon adsorbents. The isosteric heats of $CO_2$ adsorption ($Q_{st}$) for these NCs are as high as 49 kJ/mol at low $CO_2$ surface coverage, and still ~25 kJ/mol even at high $CO_2$ uptake (2.0 mmol/g), respectively. Furthermore, these NCs also exhibit high stability, excellent adsorption selectivity for $CO_2$ over $N_2$, and easy regeneration and reuse without any evident loss of $CO_2$ adsorption capacity.

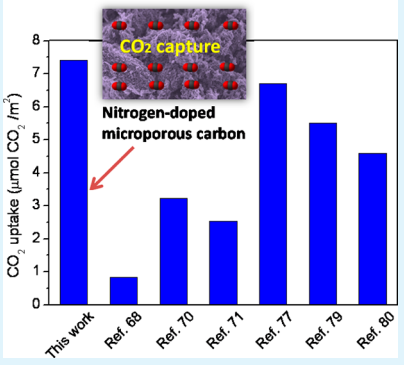


**KEYWORDS:** *microporous carbon, nitrogen doping, $CO_2$ capture, adsorption and separation*

## INTRODUCTION

$CO_2$ mainly resulting from the combustion of fossil fuels is a major greenhouse gas causing significant global climate warming. It is proposed that fossil fuels will still play a dominant role in global energy supply in the next decades, although the renewable energy production is increasing. Accordingly, the global $CO_2$ emission will further increase 40% by 2030 compared to year 2010.[1] As the strongest contributor, the fossil-fuel-fired power plants result in about 44% of $CO_2$ emission.[2] The flue gas from these plants is comprised of 70% $N_2$ and 15% $CO_2$, as well as $O_2$, water vapor, and minor impurities. To fight against global climate warming, it is important to reduce anthropogenic $CO_2$ emission from these fixed-point emission sources. Thus, there is growing interest in developing new materials and technologies with high uptakes and selectivity for efficient adsorption and separation of a large amount of $CO_2$ from these giant emission sources. In present industry, the chemical absorption−regeneration processes using aqueous amine−ammonia solutions are employed for large scale $CO_2$ separation.[3] They are efficient processes for $CO_2$ adsorption, but they have severe corrosion problems and also are highly energy-consuming because of the energy penalty necessary for regenerating aqueous amine-based solutions. Therefore, it is highly desirable to develop novel environmentally friendly materials with high adsorption capacities, $CO_2/N_2$ selectivity, and good regeneration ability for $CO_2$ capture and separation.

Alternatively, adsorption by porous solid sorbents and $CO_2$ molecules is considered to be one of the promising, sustainable technologies for capturing $CO_2$ from the flue gases. Various porous materials such as porous carbons,[4,5] zeolites,[6,7] porous silica,[8,9] porous CaO,[10,11] metal−organic frameworks (MOFs),[12,13] porous organic polymers,[14,15] etc.,[16,17] have been investigated as the sorbents for $CO_2$ adsorption and separation. Generally, these porous materials have well-defined pore structures and high specific surface areas, and thus are able to capture a large amount of $CO_2$ molecules. Furthermore, most of these materials can be modified by implementing basic sites adsorbing more acidic $CO_2$ molecules. Among these porous adsorbents widely studied in the field of $CO_2$ uptake, porous carbon materials have attracted much attention because they have many desirable advantages of variable morphologies, low cost, adjustable porosity, lightweight, easy processability, fast adsorption kinetics, high chemical and thermal stability, and

Received: January 7, 2013
Accepted: March 26, 2013
Published: March 26, 2013

  

controllable heteroatom doping.[18] Besides the field of $CO_2$ capture,[5,16] porous carbons also have great potentials in various applications such as the electrode materials in various electrochemical devices,[19−21] bioimaging,[22] catalysis,[23−28] $H_2$/methane storage,[20,29−33] etc.[34,35]

However, the adsorption interaction between $CO_2$ molecules and porous carbons depends highly on pore diameter and can be very low, resulting in poor $CO_2$ uptakes for conventional porous carbons.[36] Therefore, many efforts have been focused on enhancing the adsorption interaction and selectivity of $CO_2$ capture by increasing internal surface areas of porous carbons or introducing functional basic groups on the material surface. For example, chemical activation has been employed to develop the interconnected pore networks in carbon matrix. Using KOH as the activation reagent, the resulting activated porous carbons could possess very high specific surface areas[19] and thus good $CO_2$ adsorption capacities.[4,37,38] The impregnation or grafting of organic amines into the carbon framework formed amine functional porous carbons which could show enhanced $CO_2$ adsorption capacities. The direct heat treatment of porous carbons with ammonia at high temperatures can introduce the amine groups on the material surface.[39,40] However, these technologies including both the increase of the surface areas by the postactivation using various chemical reagents and the postintroduction of the basic amine groups suffer from several evident drawbacks such as being time-consuming and high costs. Therefore, it is highly desirable to prepare the nitrogen-incorporated porous carbons via a one-step procedure without any postmodification. Nitrogen can be doped into the carbon frameworks of porous carbons by the direct pyrolysis of the nitrogen-containing precursors at high temperatures. The nitrogen content and the microstructures (surface areas, pore volume, and pore size) of the resulting nitrogen-doped porous carbons are highly related to those of nitrogen-containing organic precursors. However, those known nitrogen-containing polymers, such as polypyrrole (15−25 $m^2/g$),[41] polyaniline (~10 $m^2/g$),[42] etc., have very low surface areas and thus they are not the ideal precursors of porous carbons obtained by pyrolysis. Subject to KOH activation, these polymers could be transformed into highly porous carbons with low yields, accompanying the production of a large amount of wastes.

In this paper, a series of nitrogen-doped porous carbons (NCs) were prepared by the direct pyrolysis of a novel high-surface-area polymer, imine-linked polymer (ILP), which was synthesized by the Schiff base condensations in DMSO under catalyst-free conditions with only water as a side product.[43] The as-prepared ILP has a high specific surface area (up to 744 $m^2/g$) and very high nitrogen contents of up to 10.21 wt %. The direct pyrolysis of the ILP at different temperatures could form the NCs with moderate surface areas (263−366 $m^2/g$), retained micropore sizes, and high nitrogen contents (5.58−8.74%). It has shown that the combination of high density nitrogen functional groups and well-defined micropore size in the NCs results in excellent $CO_2$ adsorption capacities. At 1 bar and room temperature, the calculated adsorption capacity for $CO_2$ per $m^2$ ($\mu$mol of $CO_2/m^2$) of NC-800 is 7.41 $\mu$mol of $CO_2/m^2$, the highest ever reported for porous carbon adsorbents for $CO_2$ capture. Furthermore, these NCs also exhibit high stability, high selectivity for $CO_2$ over $N_2$, and easy regeneration and reuse without any evident loss of $CO_2$ adsorption capacity.

## EXPERIMENTAL SECTION

**Material Preparation.** The starting materials and solvent were purchased from commercial sources (Sigma-Aldrich) without purification before use. Imine-linked polymer was prepared on the basis of the Schiff base chemistry using *m*-phenylenediamine and terephthalaldehyde as the starting materials. Each starting material (28.8 mmol) and dimethyl sulfoxide (DMSO, 120 mL) were added into a 300 mL round-bottom flask fitted with a water-cooled condenser and a magnetic stir bar. After degassing by argon, the mixture was heated at 180 °C overnight under magnetical stirring. After cooling down to room temperature, the solid product was separated by filtration over a Büchner funnel and washed with a large amount of ethanol. The resulting yellow powder was then dried at 80 °C for 1 day in air. The as-prepared imine-linked polymer (ILP) was transformed into nitrogen-doped porous carbons by calcination at different temperatures for 1 h with 3 °C/min under an argon gas flow (50 mL/min). The resulting porous carbons were labeled as NC-*T*, where NC is the abbreviation of nitrogen-doped porous carbon and *T* is the calcination temperature in °C.

NC-700 was further treated with concentrated HCl (37 wt %) to neutralize the nitrogen-containing basic groups. The protonated carbon was filtrated, followed by a large amount of water and ethanol until the pH of the filtrate was neutral. The final carbon, dried at 100 °C overnight, was named NC-700-HCl which was used as the control $CO_2$ adsorbent.

**Characterization.** Nitrogen adsorption isotherms were collected at −196 °C using a Quantachrome Autosorb 1C apparatus. Prior to the measurement, the samples were degassed in a vacuum at 150 °C for 16 h. Specific surface areas were calculated using the Brunauer−Emmett−Teller (BET) equation ($p/p_0$ = 0.1−0.3). The total pore volume was determined at relative pressure $p/p_0$ = 0.98. The pore size distribution was estimated according to the quenched solid density functional theory (QSDFT) equilibrium model for slit pores using the Autosorb 1.56 software from Quantachrome. The micropore surface area was calculated by the t-plot method.

X-ray powder diffraction patterns were recorded at a 2$\theta$ scan rate of 3°/min in transmission geometry using a Stoe Stadi-P diffractometer and Cu K$\alpha_1$ radiation ($\lambda$ = 0.15405 nm).

Transmission electron microscopy (TEM) investigations were performed using a 200 kV TEM FEI Tecnai T20 instrument. Scanning electron microscopy (SEM) coupled with energy dispersive X-ray analysis (EDX) was performed on a "DSM-982 Gemini" using a BSE (backscattered electron) detector from Zeiss.

Scanning electron microscopy (SEM) coupled with energy dispersive X-ray analysis (EDX) was performed on a "DSM-982 Gemini" using a BSE (backscattered electron) detector from Zeiss.

CNHS elemental analyses were performed using a EURO EA elemental analyzer, fabricated by EURO VECTOR Instruments & Software.

Thermal analysis (TGA) was performed using a Netzsch STA-409 instrument.

X-ray photoelectron spectra were recorded on a Kratos Axis Ultra DLD spectrometer equipped with a monochromatic Al KR X-ray source (75−150 W) and analyzer pass energy of 160 eV (for survey scans) or 40 eV (for detailed scans).

**$CO_2$ and $N_2$ Adsorption Experiments at 0 or 25 °C.** The $CO_2$ and $N_2$ adsorption measurements were carried out using a Quantachrome Autosorb-1 apparatus at 0 or 25 °C and up to 1 bar. Before each measurement, the sample (~100 mg) was degassed to remove any moisture and $CO_2$ molecules adsorbed in the pores at 150 °C in a vacuum for 24 h. The sample was then cooled down to 0 or 25 °C, followed by the introduction of $CO_2$ or $N_2$ into the system. To investigate the recyclability of the nitrogen-doped porous carbon in $CO_2$ capture, the used porous carbon was regenerated by evacuating at 150 °C for 1 h in a vacuum and then reused in $CO_2$ adsorption test.

## RESULTS AND DISCUSSION

As shown in Figure 1a, porous imine-linked polymer (ILP) could be efficiently prepared via Schiff base condensation of *m*-

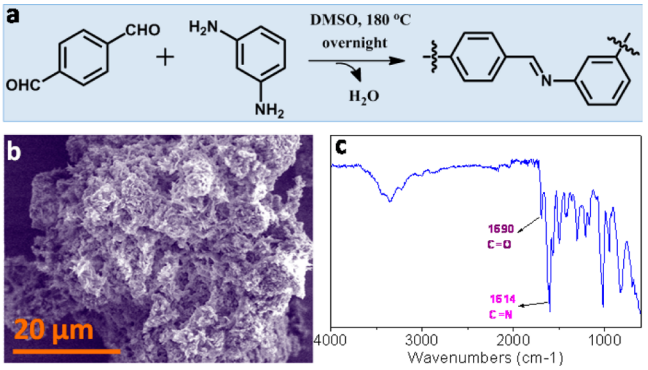


**Figure 1.** (a) Reaction equation showing the condensation between terephthalaldehyde and *m*-phenylenediamine to form imine-linked polymer (ILP). (b) SEM image and (c) FT-IR spectrum of the ILP.

phenylenediamine and terephthalaldehyde as the starting materials. This reaction took place without any catalysts, and water was released as the only side-product. Various organic solvents were suitable as the reaction media, but DMSO gave the best yield of the desired polymer with high porosity.[43] The resulting ILP is yellow powder, and the SEM image shows that it has a loose, porous structural morphology (Figure 1b). The successful preparation of ILP is proven by FT-IR (Figure 1c). A strong imine (C═N) stretch is observed at 1614 $cm^{-1}$, which confirms the presence of a large amount of imine bands in the polymer.[44] Moreover, a small band at 1690 $cm^{-1}$ ascribed to unreacted aldehydes as the end groups is also found. Some unreacted amine groups are also observed, as indicated by a broad band in the range 3200−3700 $cm^{-1}$.[45] The presence of the unreacted end groups is very common in this kind of polymer. The highly active imine functional groups in the ILP could be further transformed into novel poly(*α*-amino nitrile) frameworks containing both second amine and nitrile groups via one-pot Strecker reaction.[44,46−48]

To confirm the stability of ILP, the TG-DTG measurement was performed in an air flow. As shown in Figure 2, there are

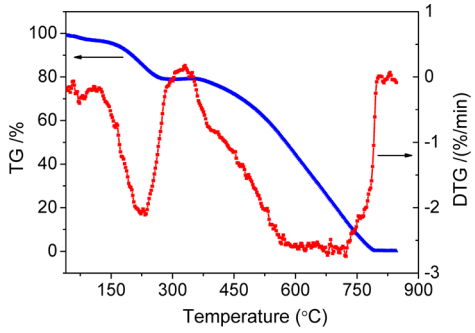


**Figure 2.** TG-DTG curves of ILP in an air flow (10 °C/min).

three weight loss stages in the TG curves. The first stage of weight loss of ∼3.5 wt % below 110 °C is attributable to the desorption of the adsorbed moisture as well as some acidic $CO_2$ molecules. The corresponding DTG curve shows a small plateau with a maximum centered at ∼76 °C. The second weight loss of ∼17.2 wt % with a plateau at ∼227 °C in the DTG curve happens between 110 and 324 °C, which should be ascribed to the evaporation of DMSO adsorbed in porous ILP. The third giant mass loss of ∼78.6 wt % between 380 and 800 °C could be ascribed to the combustion of polymer in air.[49] The final residual mass is ∼0.3 wt % at 850 °C. The result from the TG analysis indicates that the resulting ILP has a high thermal stability up to 400 °C in air. The stability of the ILP is similar to that of recently reported covalent organic polymers.[43,45,50]

After the pyrolysis at 600−800 °C in an argon flow, the ILP could be transformed into nitrogen-doped carbons (NCs). The NCs were obtained in excellent yields up to 50.1 wt %, although a little decrease was observed at increasing pyrolysis temperature (Table 1). These yields are far higher than those of

**Table 1. Yield and Textural Properties of ILP and NCs**

| sample | yield (%) | $S_{BET}$ ($m^2\ g^{-1}$) | $V_p$[a] ($cm^3\ g^{-1}$) | $S_{micro}$[b] ($m^2\ g^{-1}$) | $D_{pore}$[c] (nm) |
|---|---|---|---|---|---|
| ILP | | 744 | 0.62 | 553 | 0.86 |
| NC-600 | 50.1 | 366 | 0.43 | 259 | 0.81 |
| NC-700 | 48.5 | 284 | 0.39 | 167 | 0.81 |
| NC-800 | 47.8 | 263 | 0.38 | 155 | 0.81 |

[a]Total pore volume at $p/p_0 = 0.98$. [b]Determined by the t-plot method. [c]Maxima of the pore size distribution calculated by the QSDFT method.

activated porous carbons prepared by KOH activation of various organic polymers.[38,51] The resulting NCs demonstrate a different morphology from that of the ILP. As shown in Figure 3, SEM analysis reveals a general morphology of the aggregates

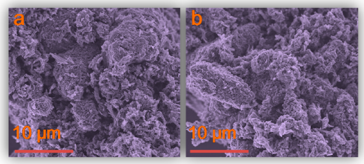


**Figure 3.** SEM images of NC-600 (a) and NC-800 (b).

of particles with different sizes, regardless of the pyrolysis temperature. The wide-angle XRD profiles of both ILP and all NCs exhibit the similar shapes without any sharp signals, indicating that they are amorphous random frameworks (Figure 4). The high-resolution TEM image discloses the absence of long-range order in NC-800 (the inset of Figure 4), matching well with that from XRD analysis.

The nitrogen adsorption measurements were performed at −196 °C to investigate the pore structure of the as-prepared

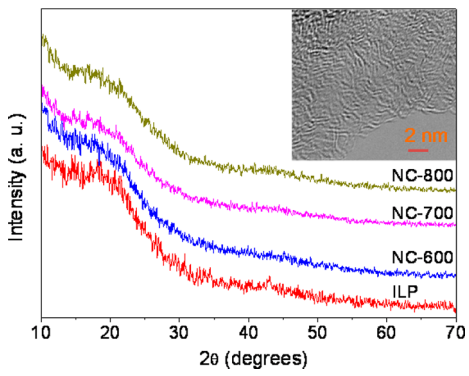


**Figure 4.** XRD patterns of ILP and NCs. The inset is a high resolution TEM image of NC-800.


dx.doi.org/10.1021/am400059t | ACS Appl. Mater. Interfaces 2013, 5, 3160−3167

ILP and NCs. The corresponding nitrogen adsorption isotherms and pore size distributions are shown in Figure 5a

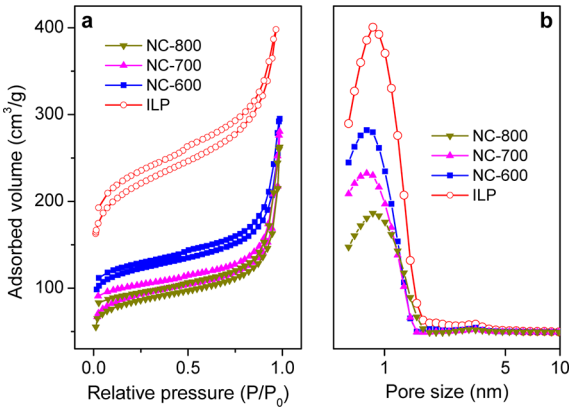


**Figure 5.** Nitrogen adsorption isotherms (a) and pore size distribution curves (b) of ILP and various nitrogen-doped porous carbons.

and b, respectively, and the textural properties are listed in Table 1. The resulting ILP shows the nitrogen adsorption isotherms with typical characteristics of microporous materials (Figure 5a). The specific surface area and pore volume of ILP are up to 744 $m^2/g$ and 0.62 $cm^3/g$, respectively. Indeed, the specific surface area in the micropore range is as high as 553 $m^2/g$ according to the t-plot method. The ILP demonstrates one single narrow micropore diameter centered at ~0.86 nm, confirmed by the pore size distribution curve (Figure 5b). The ILP-derived NCs exhibit similar nitrogen adsorption isotherms to the ILP, implying the retention of microporous structure in the NCs. However, the amount of nitrogen adsorbed evidently decreased with the rise of pyrolysis temperature. Accordingly, the specific surface area and pore volume decay from 744 $m^2/g$ (ILP) to 366 $m^2/g$ (600 °C) and 263 $m^2/g$ (800 °C) and from 0.62 $cm^3/g$ to 0.43 $cm^3/g$ (600 °C) and 0.38 $cm^3/g$ (800 °C), respectively (Table 1). All NCs have the same narrow micropore size (~0.81 nm), implying the successful maintenance of micropore size of the ILP after the pyrolysis in spite of a little reduction (Figure 4b and Table 1).

Elemental analyses (Table 2) revealed that the ILP contained 66.75 wt % carbon, 10.21 wt % nitrogen, 8.22 wt % sulfur, and

**Table 2. CNHS Chemical Elemental Analysis of ILP and Various NCs**

| sample | N (wt %) | C (wt %) | S (wt %) | H (wt %) |
|---|---|---|---|---|
| ILP | 10.21 | 66.75 | 8.22 | 5.36 |
| NC-600 | 8.74 | 82.76 | 0.37 | 2.36 |
| NC-700 | 6.82 | 84.15 | 1.70 | 1.26 |
| NC-800 | 5.58 | 86.42 | 1.62 | 0.85 |

5.36 wt % hydrogen. The presence of sulfur in the ILP should be derived from the solvent DMSO used during the preparation of the ILP. And the content of DMSO calculated according to the result of elemental analysis is ~20 wt %, comparable to that (17.2 wt %) obtained by TG analysis. The good ability of storing high-content DMSO should be the result of the high specific surface area of porous ILP. After the pyrolysis, it can be seen that the nitrogen and hydrogen content gradually decrease with increasing pyrolysis temperature from 10.21 wt % (ILP) to 5.58 wt % (800 °C) and from 5.36 wt % (ILP) to 0.85 wt % (800 °C), respectively. The pyrolysis at high temperature can result in the loss of heteroatoms in porous carbons.[52] NC-600 has a large amount of nitrogen up to 8.74 wt % which is one of the highest nitrogen contents reported for porous carbons. Interestingly, the chemical elemental analysis showed that the final NCs are also sulfur-containing. It is believed that the introduction of sulfur is realized by the surface reaction of polymer and DMSO at high temperature. The sulfur content of NC-600 is only 0.37 wt %, and it evidently increases to 1.70 wt % for NC-700 and 1.62 wt % for NC-800, respectively. It has been proposed that the sulfur doping into microporous carbons is advantageous to enhance $CO_2$ adsorption performance because of the enhanced interaction of $CO_2$ molecules with the material surface.[53] Thus, the incorporation of sulfur as well as high density basic nitrogen-containing groups in the NCs should improve their $CO_2$ adsorption capacities.

X-ray photoelectron spectroscopy (XPS) is used to further study the nature of functional groups on the surface of the ILP and NCs. The XP survey spectra show the presence of three distinct peaks and one weak peak ascribed to carbon, nitrogen, oxygen, and sulfur, respectively (Supporting Information, Figure S1). Quantitative elemental analysis by XPS indicates that ILP, NC-600, NC-700, and NC-800 contain 10.56, 8.39, 6.65, and 5.63% nitrogen, respectively (Supporting Information, Table S2). These values are very close to those obtained by CNHS chemical elemental analysis, indicating that the concentrations of the surface nitrogen-containing functional groups in the ILP and NCs are similar to the concentrations of nitrogen groups in the bulk. The N 1s and C 1s core level spectra of the ILP and various NCs prepared by carbonization of the ILP at temperatures of 600−800 °C are presented in Figure 6. As shown in Figure 6a, The ILP only demonstrates

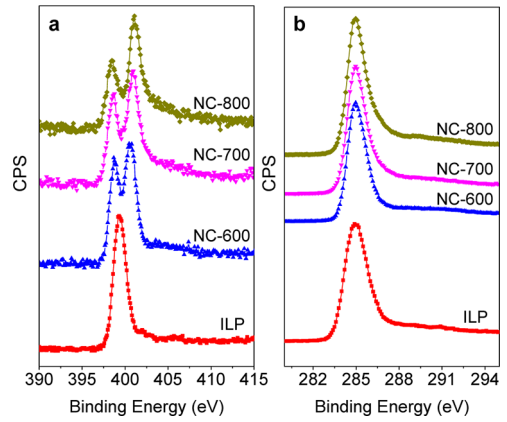


**Figure 6.** N 1s (a) and C 1s (b) XPS spectra of the as-prepared ILP and various NCs.

one peak at ~399.4 eV due to a single nitrogen-containing functional group of the pyridine type.[54,55] The pyrolysis at high temperatures resulted in different N 1s peaks (Figure 6a), indicating the decomposition of the ILP and the formation of new nitrogen species. The binding energy of the pyridine-type nitrogen in the NCs is 398.7 eV, which is a further shift of 0.7 eV to lower binding energies. This shift in binding energy of the pyridine-type nitrogen in the NCs compared to the ILP should be ascribed to the enhanced surface interaction. Another peak at 400.9 eV in the N 1s spectra of the NCs corresponds to the quaternary N,[56] which is the most stable nitrogen group in the nitrogen-doped carbons prepared by the pyrolysis. The strength in binding energy of the quaternary N evidently increases


dx.doi.org/10.1021/am400059t | ACS Appl. Mater. Interfaces 2013, 5, 3160−3167

compared to that of the pyridine type N as the pyrolysis temperature, showing more and more nitrogen species are strongly buried in the carbon matrix.[57,58] As presented in Figure 6b, the C 1s signals of the ILP and NCs appear at about 285.0 eV, which is consistent with graphene $sp^2$ carbon. In all spectra, there is a clear shoulder between 285.2 and 289.0 eV,[59,60] which can be due to carbon bound to nitrogen/sulfur/oxygen on the material surfaces. The existence of small amounts of sulfur in the NCs is also confirmed by XPS analysis, as shown in Figure S2 in the Supporting Information. The S 2p signals in all NCs are split into two main peaks which are at 164.1 and 165.2 eV, respectively. Both peaks correspond to spin−orbit splitting of sulfur atoms doped into graphene sheets. It means that the sulfur atoms have incorporated into the carbon framework via the formation of the C−S band.[61,62]

The as-prepared ILP and NCs were further used as adsorbents for $CO_2$ capture considering their features of basic nitrogen groups and narrow uniform micropores. At pressures up to 1 bar, the $CO_2$ adsorption isotherms of the ILP and NCs collected at 25 and 0 °C, respectively, are shown in Figure 7

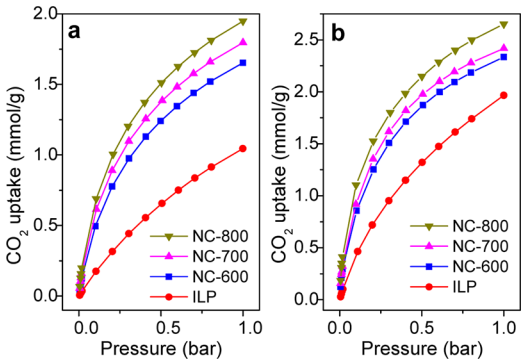


**Figure 7.** $CO_2$ adsorption isotherms of polyimine and various NCs at 25 °C (a) and 0 °C (b), respectively.

and Figure S3−6 (Supporting Information), and the adsorption uptakes are presented in Table S2 (Supporting Information). At 1 bar, porous ILP shows moderate $CO_2$ uptakes of 1.05 mmol/g (46.2 mg/g) and 1.97 mmol/g (86.7 mg/g) at 25 and 0 °C, respectively, which are comparable to the recently reported ones of various organic porous polymers.[14,15,63] As shown in Figure 6, it can be seen that the transformation of porous ILP to the NCs obtained by the pyrolysis can evidently increase the $CO_2$ adsorption capacities, possibly because of both the narrower micropore sizes and more specific surface sites in the NCs. At 1 bar, NC-600 pyrolyzed at 600 °C has $CO_2$ uptakes of 1.65 and 2.33 mmol/g at 25 and 0 °C, respectively, significantly higher than the ILP. Further increase in the pyrolysis temperature could result in a little higher $CO_2$ adsorption capacities, and the highest uptakes of $CO_2$ capture for NC-800 are 1.95 and 2.65 mmol/g at 25 and 0 °C, respectively. As shown in Table S3 (Supporting Information), NC-800 has a low specific surface area of 263 $m^2/g$, but its $CO_2$ adsorption capacity evidently outperforms graphitic nanofibers (1.3 mmol/g at 25 °C),[64] nanoporous melamine resin sponges (1.6 mmol/g at 0 °C),[14] resin-based carbons (1.86 mmol/g at 25 °C),[39] and conjugated microporous polymers (1.45 mmol/g at 25 °C).[15] The $CO_2$ adsorption capacities of NC-800 are also compared to those of various porous carbon materials with high surface areas of over 1000 $m^2/g$, such as widely used activated carbons (~2 mmol/g at 25 °C),[31] hard-templated CMK-3 (2.2 mmol/g at 25 °C) and CMK-8 (2.1 mmol/g at 25 °C),[4] and nitrogen-doped hierarchical porous carbons (2.2 mmol/g at 25 °C).[65]

In order to further determine the interaction strength between $CO_2$ molecules and the surface of the NCs, the isosteric heat of adsorption ($Q_{st}$) was calculated from the $CO_2$ adsorption isotherms at 273 and 298 K on the basis of the Clausius−Clapeyron equation.[66] The plots as a function of $CO_2$ uptake for the as-prepared NCs are shown in Figure S7 (Supporting Information). The $Q_{st}$ values for the NCs are in the range 45−49 kJ/mol at low $CO_2$ uptake, which are higher than those reported for nitrogen-doped templated carbons from zeolite and mesoporous silica (31−36 kJ/mol),[67,68] spherical nitrogen-doped microporous carbons (30 kJ/mol),[69] nitrogen-incorporated hierarchical porous carbons (33−37 kJ/mol),[65,70] and triptycene-derived benzimidazole-linked polymers (29 kJ/mol).[71] The high $Q_{st}$ values indicate that the NCs strongly interact with acidic $CO_2$ molecules. It is worth noting that NC-800 has the lower $Q_{st}$ value of 45 kJ/mol than NC-600 and NC-700, but it has the highest $CO_2$ uptakes among these NCs. It implies that the nature of the adsorption is physical adsorption which strongly depends on the pore structure of porous carbons. Furthermore, the $Q_{st}$ values for the NCs at low surface coverage clearly decrease as the nitrogen contents of the carbons, indicating that the nitrogen functional groups play an important role for $CO_2$ capture. The $Q_{st}$ values evidently decrease to 22−25 kJ/mol as the $CO_2$ uptake increases, implying that two $CO_2$ adsorption mechanisms coexist in these NCs; $CO_2$ molecules are adsorbed onto both the nitrogen functional groups and the nondoped porous carbon surface. Among these NCs, NC-600 has the highest $Q_{st}$ of 25 kJ/mol at higher coverage (2.0 mmol/g), which are higher than biomass-derived porous carbons (22 kJ/mol at 0.7 mmol/g)[72] and porous polyamine (18 kJ/mol at 2.2 mmol/g),[73] since NC-600 has both high nitrogen contents and textural properties. Furthermore, it has been reported that the undoped porous carbons have a $Q_{st}$ value of about 17 kJ/mol at high surface coverage, which is evidently lower than our values (22−25 kJ/mol) for the NCs. All these data above demonstrate the importance of introducing basic nitrogen functional groups onto porous carbons in increasing $CO_2$ uptake.

As shown in Figure 8 and Table S4 (Supporting Information), the adsorption capacities for $CO_2$ per $m^2$

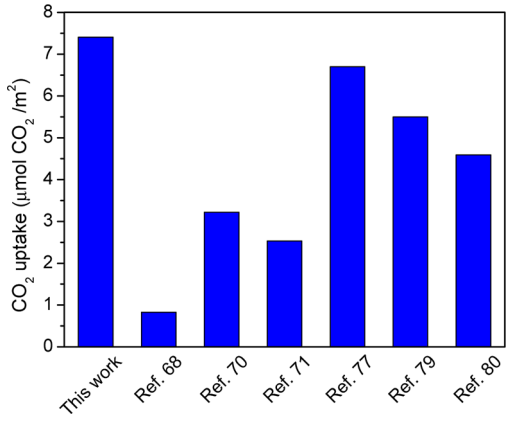


**Figure 8.** The comparison of $CO_2$ adsorption capacities for NC-800 in this work and several recently reported porous carbon adsorbents. The $CO_2$ adsorption capacities were collected at 1 bar and 25 °C.

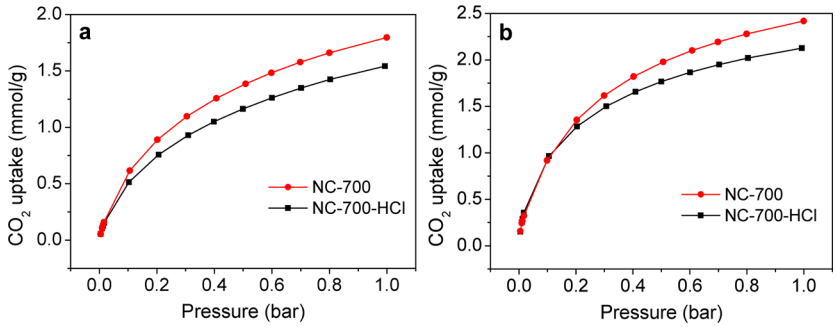


**Figure 9.** $CO_2$ adsorption isotherms of NC-700 and NC-700-HCl at 25 °C (a) and 0 °C (b), respectively.

($\mu$mol of $CO_2/m^2$) of NC-800 were also compared with those of various recently reported adsorbents for $CO_2$ capture. At 1 bar and 25 °C, NC-800 demonstrates 7.41 $\mu$mol of $CO_2/m^2$, which is one of the best values reported for $CO_2$ capture using various adsorbents. For example, various nitrogen-doped porous carbons prepared using different procedures only gave poor to moderate $CO_2$ adsorption capacities of 1.31−6.70 $\mu$mol of $CO_2/m^2$,[67,69,70,74−77] evidently lower than our reported value (7.41 $\mu$mol of $CO_2/m^2$) for NC-800. Polyacrylonitrile-based activated carbon fibers only showed poor $CO_2$ adsorption capacities of 1.97 $\mu$mol of $CO_2/m^2$.[78] Self-assembly of poly(benzoxazine-*co*-resol) in combination with a carbonization process formed a nitrogen-containing carbon framework, showing $CO_2$ adsorption capacities of 5.50 $\mu$mol of $CO_2/m^2$.[79] Porous carbons derived from melamine−formaldehyde had 4.59 $\mu$mol of $CO_2/m^2$.[80] The introduction of sulfur into the framework of microporous carbon only showed 1.54 $\mu$mol of $CO_2/m^2$.[53] The doping of CaO in mesoporous carbon resulted in moderate $CO_2$ adsorption capacities of 4.73 $\mu$mol of $CO_2/m^2$.[81] The $CO_2$ adsorption capacity of the NCs also outperforms the recently reported triptycene-derived benzimidazole-linked polymers (2.53 $\mu$mol of $CO_2/m^2$).[71] The nanostructured carbon prepared using zeolite Y as the hard template only showed 0.83 $\mu$mol of $CO_2/m^2$.[68] KOH activation of carbon-based materials is an efficient method for forming microporous carbons with enhanced surface areas, thus resulting in increased gas storage capacities.[19] By activation of yeast or fungi based carbons using KOH, the resulting microporous carbons showed poor to moderate $CO_2$ adsorption capacities of 1.55−3.45 $\mu$mol of $CO_2/m^2$.[82,83] The adsorption capacity (1.85 $\mu$mol of $CO_2/m^2$)[40] of Olive stones-based carbon activated by $CO_2$ also did not outperform the NCs prepared by us. By selecting etching of silicon elements in carbide materials using chlorine at high temperature,[33] the as-prepared carbide-derived carbons had very high specific surface areas and the maximum $CO_2$ adsorption capacity was 3.87 $\mu$mol of $CO_2/m^2$, only half of our value for NC-800.[5] The high density of $CO_2$ molecules adsorbed on the surface of NC-800 is ascribed to the uniform micropore sizes as well as high contents of basic nitrogen functional groups.

Yashima and his co-workers reported that the basic nitrogen-containing groups could efficiently act as the anchor sites for $CO_2$ capture.[84] Thus, it is believed that not only a large amount of micropores but also surface basic nitrogen groups can contribute to good adsorption capacities for $CO_2$ capture of the NCs. To investigate the effect of the basic nitrogen functional groups on the $CO_2$ adsorption capacity, the basic nitrogen groups in the NCs were first neutralized by concentrated HCl and then we measured the $CO_2$ adsorption isotherms of the resulting NC-700-HCl at 25 and 0 °C, respectively. As indicated in Figure 9, the $CO_2$ uptakes at 1 bar of NC-700-HCl are only 1.54 and 2.13 mmol/g at 25 and 0 °C, respectively. Both $CO_2$ capture values are evidently lower than those of NC-700 (1.80 mmol/g at 25 °C and 2.42 mmol/g at 0 °C, respectively). This comparison clearly shows that acid treatment results in 12−15% $CO_2$ uptake loss of total $CO_2$ adsorption capacities, which is a result of the neutralization of basic nitrogen sites by acid. Thus, the existence of the basic nitrogen groups in the NCs could enhance the $CO_2$ capture capacities of porous carbons.

For practical applications, porous carbons should also show easy regeneration, high stability and recyclability, and high selectivity for $CO_2$ over $N_2$ beyond good $CO_2$ uptakes. Figure S8 (Supporting Information) displays $CO_2$ adsorption isotherms for NC-800 at 0 °C of five repeated runs with regeneration. The $CO_2$ uptakes at 1 bar are similar under the same conditions within five repeated runs, and there is no noticeable change. During the adsorption measurements, it is found that the captured $CO_2$ in the NCs can be quickly desorbed after the gas is changed from $CO_2$ to He. These results show that the NCs are very stable, and can be recycled to capture $CO_2$ without any clear loss of performance. Moreover, based on the initial slopes of $CO_2$ and $N_2$ adsorption isotherms, the estimated adsorption selectivity for $CO_2$ over $N_2$ of NC-800 is 21.6 (Supporting Information, Figure S9). This selectivity is comparable to those of PCPs[85] and poly(benzoxazine-*co*-resol)-based PCs.[79] Furthermore, the NCs show large differences in adsorption capacities between $CO_2$ and $N_2$ at 1 bar. For example, NC-800 has $N_2$ uptakes of 0.35 and 0.55 mmol/g at 25 and 0, respectively (Supporting Information, Figure S10−11), which are only about 20% of the adsorption capacities for $CO_2$ under the same conditions (Supporting Information, Figure S4). All of this data implies that the NCs prepared by the direct pyrolysis of the ILP are well selective for capturing $CO_2$ over $N_2$.

## CONCLUSIONS

Summarizing, imine-linked polymer (ILP) was successfully prepared using the commercial starting materials based on the Schiff base condensation under catalyst-free conditions. The as-prepared ILP is microporous and loose powder, exhibiting a high specific surface area of over 700 $m^2/g$ and nitrogen content of up to 10%. By direct pyrolysis of the ILP at temperatures of 600−800 °C, a series of nitrogen-doped porous carbons (NCs) was formed with moderate specific surface areas of up to 366 $m^2/g$, pore volumes of 0.43 $cm^3/g$, and narrow micropore size distributions. The resulting NCs contain not only variable nitrogen contents (5.58−8.74%) but also different


dx.doi.org/10.1021/am400059t | ACS Appl. Mater. Interfaces 2013, 5, 3160−3167

sulfur contents (0.37−1.7%) depending on the pyrolysis temperatures. The doping of sulfur in the NCs is ascribed to the surface reaction of the ILP and DMSO adsorbed in the ILP at high temperatures.

The as-prepared NCs as well as their precursor (ILP) were investigated in $CO_2$ capture considering their microporous textural properties and high contents of basic nitrogen groups. At 1 bar, porous ILP shows moderate $CO_2$ uptakes of 1.05 mmol/g (46.2 mg/g) and 1.97 mmol/g (86.7 mg/g) at 25 and 0 °C, respectively. The pyrolysis of the ILP at high temperatures can evidently increase the $CO_2$ adsorption capacities because of the narrower micropore sizes in the NCs. Among the tested porous materials, at 1 bar, NC-800 prepared by the pyrolysis of the ILP at 800 °C showed the highest $CO_2$ uptakes of 1.95 and 2.65 mmol/g at 25 and 0 °C, respectively. The calculated adsorption capacity for $CO_2$ per $m^2$ ($\mu$mol of $CO_2/m^2$) of NC-800 is 7.41 $\mu$mol of $CO_2/m^2$ at 1 bar and 25 °C, which is the biggest value among various reported physisorbents for $CO_2$ capture. Furthermore, these NCs also exhibit high stability, large $CO_2/N_2$ adsorption ratio of up to 5, excellent adsorption selectivity (21.6) for $CO_2$ over $N_2$, and easy regeneration and reuse without any evident loss of $CO_2$ adsorption capacity. Thus, the NCs derived from the ILP have great potential applications as the selective adsorbents for $CO_2$ and $N_2$ separation in flue gas of power plants burning fossil fuels.

## ■ ASSOCIATED CONTENT

### Supporting Information

Figures showing XPS spectra and $CO_2$ and $N_2$ adsorption isotherms of ILP and NCs; tables showing elemental composition of ILP and NCs determined by XPS analysis, $CO_2$ uptakes for ILP, NCs and NC-700-HCl, and the comparison of NC-800 with recently reported porous carbons. This material is available free of charge via the Internet at http://pubs.acs.org.

## ■ AUTHOR INFORMATION

### Corresponding Author

*E-mail: jiacheng.wang@mail.sic.ac.cn (J.W.). Fax: +86 21 52412404 (J.W.). Phone: +86 21 52412714 (J.W.); stefan.kaskel@chemie.tu-dresden.de (S.K.). Fax: +49 351 46337287 (S.K.). Phone: +49 351 46334885 (S.K.).

### Notes

The authors declare no competing financial interest.

## ■ ACKNOWLEDGMENTS

J.W. thanks the Alexander von Humboldt Foundation for granting him a research fellowship. This work is also financially supported by Shanghai Institute of Ceramics, the One Hundred Talent Plan of Chinese Academy of Sciences. The authors are highly thankful to Dr. David Morgan in Department of Chemistry, Cardiff University, for performing the XPS measurements.

## ■ REFERENCES

(1) Sridhar, S.; Smitha, B.; Aminabhavi, T. *Sep. Purif. Rev.* **2007**, *36*, 113−174.
(2) Yu, K. M. K.; Curcic, I.; Gabriel, J.; Tsang, S. C. E. *ChemSusChem* **2008**, *1*, 893−899.
(3) Häring, H.-W.; Ahner, C. *Industrial Gases Processing*; Wiley-VCH: Weinheim, Germany, 2008.
(4) Sevilla, M.; Fuertes, A. B. *J. Colloid Interface Sci.* **2012**, *366*, 147−154.
(5) Presser, V.; McDonough, J.; Yeon, S.-H.; Gogotsi, Y. *Energy Environ. Sci.* **2011**, *4*, 3059−3066.
(6) Kusakabe, K.; Kuroda, T.; Morooka, S. *J. Membr. Sci.* **1998**, *148*, 13−23.
(7) Fang, H.; Kamakoti, P.; Zang, J.; Cundy, S.; Paur, C.; Ravikovitch, P. I.; Sholl, D. S. *J. Phys. Chem. C* **2012**, *116*, 10692−10701.
(8) Fauth, D.; Gray, M.; Pennline, H.; Krutka, H.; Sjostrom, S.; Ault, A. *Energy Fuels* **2012**, *26*, 2483−2496.
(9) Seo, Y. T.; Moudrakovski, I. L.; Ripmeester, J. A.; Lee, J.; Lee, H. *Environ. Sci. Technol.* **2005**, *39*, 2315−2319.
(10) Abanades, J. C.; Anthony, E. J.; Lu, D. Y.; Salvador, C.; Alvarez, D. *AIChE J.* **2004**, *50*, 1614−1622.
(11) Broda, M.; Müller, C. R. *Adv. Mater.* **2012**, *24*, 3059−3064.
(12) Senkovska, I.; Hoffmann, F.; Fröba, M.; Getzschmann, J.; Böhlmann, W.; Kaskel, S. *Microporous Mesoporous Mater.* **2009**, *122*, 93−98.
(13) Debatin, F.; Thomas, A.; Kelling, A.; Hedin, N.; Bacsik, Z.; Senkovska, I.; Kaskel, S.; Junginger, M.; Müller, H.; Schilde, U. *Angew. Chem., Int. Ed.* **2010**, *49*, 1258−1262.
(14) Wilke, A.; Weber, J. *J. Mater. Chem.* **2011**, *21*, 5226−5229.
(15) Ren, S.; Dawson, R.; Laybourn, A.; Jiang, J.-X.; Khimyak, Y.; Adams, D. J.; Cooper, A. I. *Polym. Chem.* **2012**, *3*, 928−934.
(16) Wang, Q.; Luo, J.; Zhong, Z.; Borgna, A. *Energy Environ. Sci.* **2011**, *4*, 42−55.
(17) Banerjee, R.; Furukawa, H.; Britt, D.; Knobler, C.; O'Keeffe, M.; Yaghi, O. M. *J. Am. Chem. Soc.* **2009**, *131*, 3875−3877.
(18) Morris, R. E.; Wheatley, P. S. *Angew. Chem., Int. Ed.* **2008**, *47*, 4966−4981.
(19) Wang, J.; Kaskel, S. *J. Mater. Chem.* **2012**, *22*, 23710−23725.
(20) Oschatz, M.; Kockrick, E.; Rose, M.; Borchardt, L.; Klein, N.; Senkovska, I.; Freudenberg, T.; Korenblit, Y.; Yushin, G.; Kaskel, S. *Carbon* **2010**, *48*, 3987−3992.
(21) Rose, M.; Korenblit, Y.; Kockrick, E.; Borchardt, L.; Oschatz, M.; Kaskel, S.; Yushin, G. *Small* **2011**, *7*, 1108−1117.
(22) Yang, S.; Zeng, H.; Zhao, H.; Zhang, H.; Cai, W. *J. Mater. Chem.* **2011**, *21*, 4432−4436.
(23) Joo, S. H.; Choi, S. J.; Oh, I.; Kwak, J.; Liu, Z.; Terasaki, O.; Ryoo, R. *Nature* **2001**, *412*, 169−172.
(24) Sankar, M.; Nowicka, E.; Tiruvalam, R.; He, Q.; Taylor, S. H.; Kiely, C. J.; Bethell, D.; Knight, D. W.; Hutchings, G. J. *Chem.—Eur. J.* **2011**, *17*, 6524−6532.
(25) Krawiec, P.; Kockrick, E.; Borchardt, L.; Geiger, D.; Corma, A.; Kaskel, S. *J. Phys. Chem. C* **2009**, *113*, 7755−7761.
(26) Borchardt, L.; Hasché, F.; Lohe, M. R.; Oschatz, M.; Schmidt, F.; Kockrick, E.; Ziegler, C.; Lescouet, T.; Bachmatiuk, A.; Büchner, B.; Farrusseng, D.; Strasser, P.; Kaskel, S. *Carbon* **2012**, *50*, 1861−1870.
(27) Wang, H.; Maiyalagan, T.; Wang, X. *ACS Catal.* **2012**, *2*, 781−794.
(28) Upare, D.; Yoon, S.; Lee, C. *Kor. J. Chem. Eng.* **2011**, *28*, 731−743.
(29) Yushin, G.; Dash, R.; Jagiello, J.; Fischer, J. E.; Gogotsi, Y. *Adv. Funct. Mater.* **2006**, *16*, 2288−2293.
(30) Yeon, S.-H.; Knoke, I.; Gogotsi, Y.; Fischer, J. E. *Microporous Mesoporous Mater.* **2010**, *131*, 423−428.
(31) Himeno, S.; Komatsu, T.; Fujita, S. *J. Chem. Eng. Data* **2005**, *50*, 369−376.
(32) Kockrick, E.; Schrage, C.; Borchardt, L.; Klein, N.; Rose, M.; Senkovska, I.; Kaskel, S. *Carbon* **2010**, *48*, 1707−1717.
(33) Wang, J.; Oschatz, M.; Biemelt, T.; Borchardt, L.; Senkovska, I.; Lohe, M. R.; Kaskel, S. *J. Mater. Chem.* **2012**, *22*, 23893−23899.
(34) Oschatz, M.; Borchardt, L.; Thommes, M.; Cychosz, K. A.; Senkovska, I.; Klein, N.; Frind, R.; Leistner, M.; Presser, V.; Gogotsi, Y.; Kaskel, S. *Angew. Chem., Int. Edit.* **2012**, *51*, 7577−7580.
(35) Zhu, Y.; He, X. *J. Chem.* **2013**, DOI: 10.1155/2013/530143.
(36) Wahby, A.; Ramos-Fernández, J. M.; Martínez-Escandell, M.; Sepúlveda-Escribano, A.; Silvestre-Albero, J.; Rodríguez-Reinoso, F. *ChemSusChem* **2010**, *3*, 974−981.

(37) Sevilla, M.; Alam, N.; Mokaya, R. *J. Phys. Chem. C* **2010**, *114*, 11314−11319.
(38) Sevilla, M.; Valle-Vigón, P.; Fuertes, A. B. *Adv. Funct. Mater.* **2011**, *21*, 2781−2787.
(39) Drage, T. C.; Arenillas, A.; Smith, K. M.; Pevida, C.; Piippo, S.; Snape, C. E. *Fuel* **2007**, *86*, 22−31.
(40) Plaza, M. G.; Pevida, C.; Arias, B.; Fermoso, J.; Casal, M. D.; Martin, C. F.; Rubiera, F.; Pis, J. J. *Fuel* **2009**, *88*, 2442−2447.
(41) Chao, T. H.; March, J. *J. Polym. Sci., Polym. Chem.* **1988**, *26*, 743−753.
(42) Taguchi, S.; Tanaka, T. *J. Power Sources* **1987**, *20*, 249−252.
(43) Pandey, P.; Katsoulidis, A. P.; Eryazici, I.; Wu, Y. Y.; Kanatzidis, M. G.; Nguyen, S. T. *Chem. Mater.* **2010**, *22*, 4974−4979.
(44) Wang, J. C.; Masui, Y.; Onaka, M. *Polym. Chem.* **2012**, *3*, 865−867.
(45) Uribe-Romo, F. J.; Hunt, J. R.; Furukawa, H.; Klock, C.; O'Keeffe, M.; Yaghi, O. M. *J. Am. Chem. Soc.* **2009**, *131*, 4570−4571.
(46) Wang, J. C.; Masui, Y.; Onaka, M. *Eur. J. Org. Chem.* **2010**, *2010*, 1763−1771.
(47) Strecker, A. *Ann. Chem. Pharm.* **1850**, *75*, 27−45.
(48) Wang, J. C.; Masui, Y.; Onaka, M. *Tetrahedron Lett.* **2012**, *53*, 1978−1981.
(49) Wang, J.; Yu, X.; Li, Y.; Liu, Q. *J. Phys. Chem. C* **2007**, *111*, 18073−18077.
(50) Cote, A. P.; Benin, A. I.; Ockwig, N. W.; O'Keeffe, M.; Matzger, A. J.; Yaghi, O. M. *Science* **2005**, *310*, 1166−1170.
(51) Sevilla, M.; Mokaya, R.; Fuertes, A. B. *Energy Environ. Sci.* **2011**, *4*, 2930−2936.
(52) Wang, J.; Liu, Q. *J. Phys. Chem. C* **2007**, *111*, 7266−7272.
(53) Xia, Y.; Zhu, Y.; Tang, Y. *Carbon* **2012**, *50*, 5543−5553.
(54) Greczynski, G.; Johansson, N.; Logdlund, M.; Pettersson, L. A. A.; Salaneck, W. R.; Horsburgh, L. E.; Monkman, A. P.; dos Santos, D. A.; Bredas, J. L. *J. Chem. Phys.* **2001**, *114*, 4243−4252.
(55) Cohen, M. R.; Merrill, R. P. *Surf. Sci.* **1991**, *245*, 1−11.
(56) Wang, Y.; Su, F.; Wood, C. D.; Lee, J. Y.; Zhao, X. S. *Ind. Eng. Chem. Res.* **2008**, *47*, 2294−2300.
(57) Kundu, S.; Xia, W.; Busser, W.; Becker, M.; Schmidt, D. A.; Havenith, M.; Muhler, M. *Phys. Chem. Chem. Phys.* **2010**, *12*, 4351−4359.
(58) Hunter, C. A.; Sanders, J. K. M. *J. Am. Chem. Soc.* **1990**, *112*, 5525−5534.
(59) Sanchez-Lopez, J. C.; Donnet, C.; Lefebvre, F.; Fernandez-Ramos, C.; Fernandez, A. *J. Appl. Phys.* **2001**, *90*, 675−681.
(60) Marton, D.; Boyd, K. J.; Albayati, A. H.; Todorov, S. S.; Rabalais, J. W. *Phys. Rev. Lett.* **1994**, *73*, 118−121.
(61) Kelemen, S. R.; Afeworki, M.; Gorbaty, M. L.; Sansone, M.; Kwiatek, P. J.; Walters, C. C.; Freund, H.; Siskin, M.; Bence, A. E.; Curry, D. J.; Solum, M.; Pugmire, R. J.; Vandenbroucke, M.; Leblond, M.; Behar, F. *Energy Fuels* **2007**, *21*, 1548−1561.
(62) Glenis, S.; Nelson, A. J.; Labes, M. M. *J. Appl. Phys.* **1999**, *86*, 4464−4466.
(63) Furukawa, H.; Yaghi, O. M. *J. Am. Chem. Soc.* **2009**, *131*, 8875−8883.
(64) Meng, L.-Y.; Park, S.-J. *J. Colloid Interface Sci.* **2010**, *352*, 498−503.
(65) Gutierrez, M. C.; Carriazo, D.; Ania, C. O.; Parra, J. B.; Ferrer, M. L.; del Monte, F. *Energy Environ. Sci.* **2011**, *4*, 3535−3544.
(66) Gogotsi, Y.; Portet, C.; Osswald, S.; Simmons, J. M.; Yildirim, T.; Laudisio, G.; Fischer, J. E. *Int. J. Hydrogen Energy* **2009**, *34*, 6314−6319.
(67) Zhao, Y.; Zhao, L.; Yao, K. X.; Yang, Y.; Zhang, Q.; Han, Y. *J. Mater. Chem.* **2012**, *22*, 19726−19731.
(68) Wang, L.; Yang, R. T. *J. Phys. Chem. C* **2011**, *116*, 1099−1106.
(69) Liu, L.; Deng, Q.-F.; Ma, T.-Y.; Lin, X.-Z.; Hou, X.-X.; Liu, Y.-P.; Yuan, Z.-Y. *J. Mater. Chem.* **2011**, *21*, 16001−16009.
(70) Chen, C.; Kim, J.; Ahn, W.-S. *Fuel* **2012**, *95*, 360−364.
(71) Rabbani, M. G.; Reich, T. E.; Kassab, R. M.; Jackson, K. T.; El-Kaderi, H. M. *Chem. Commun.* **2012**, *48*, 1141−1143.
(72) Sevilla, M.; Fuertes, A. B. *Energy Environ. Sci.* **2011**, *4*, 1765−1771.
(73) Wang, H.-B.; Jessop, P. G.; Liu, G. *ACS Macro Lett.* **2012**, *1*, 944−948.
(74) Xia, Y.; Mokaya, R.; Walker, G. S.; Zhu, Y. *Adv. Energy Mater.* **2011**, *1*, 678−683.
(75) Zhang, Z.; Wang, K.; Atkinson, J. D.; Yan, X.; Li, X.; Rood, M. J.; Yan, Z. *J. Hazard. Mater.* **2012**, *229−230*, 183−191.
(76) Zhou, J.; Li, W.; Zhang, Z.; Xing, W.; Zhuo, S. *RSC Adv.* **2012**, *2*, 161−167.
(77) Hao, G.-P.; Li, W.-C.; Qian, D.; Lu, A.-H. *Adv. Mater.* **2010**, *22*, 853−857.
(78) Shen, W.; Zhang, S.; He, Y.; Li, J.; Fan, W. *J. Mater. Chem.* **2011**, *21*, 14036−14040.
(79) Hao, G.-P.; Li, W.-C.; Qian, D.; Wang, G.-H.; Zhang, W.-P.; Zhang, T.; Wang, A.-Q.; Schueth, F.; Bongard, H.-J.; Lu, A.-H. *J. Am. Chem. Soc.* **2011**, *133*, 11378−11388.
(80) Pevida, C.; Drage, T. C.; Snape, C. E. *Carbon* **2008**, *46*, 1464−1474.
(81) Wu, Z.; Hao, N.; Xiao, G.; Liu, L.; Webley, P.; Zhao, D. *Phys. Chem. Chem. Phys.* **2011**, *13*, 2495−2503.
(82) Shen, W.; He, Y.; Zhang, S.; Li, J.; Fan, W. *ChemSusChem* **2012**, *5*, 1274−1279.
(83) Wang, J.; Heerwig, A.; Lohe, M. R.; Oschatz, M.; Borchardt, L.; Kaskel, S. *J. Mater. Chem.* **2012**, *22*, 13911−13913.
(84) Hiyoshi, N.; Yogo, K.; Yashima, T. *Microporous Mesoporous Mater.* **2005**, *84*, 357−365.
(85) Nakagawa, K.; Tanaka, D.; Horike, S.; Shimomura, S.; Higuchi, M.; Kitagawa, S. *Chem. Commun.* **2010**, *46*, 4258−4260.